Chapter 5
Seismotectonics of the 2013 Lushan M_w 6.7 Earthquake—A Hidden Earthquake

Ren-Qi Lu, Xi-Wei Xu, Deng-Fa He, John Suppe, Xi-Bin Tan, Ying-Qiang Li, and Zhen-Nan Wang

Abstract Almost five years after the devastating May 12, 2008, M_w 7.9 Wenchuan earthquake, southern Longmen Shan was struck by the M_w 6.7 Lushan earthquake on April 20, 2013. After the Lushan earthquake, it was debated whether the fault was a high-angle outcrop fault or a low-angle blind fault. The geometry, kinematics, and seismotectonic model of this earthquake has also been debated widely. In our study, several high-resolution artificial seismic reflection profiles are combined with near-surface geological data and well-drilling data to determine the sedimentary and structural deformation of the Lushan area. Our study integrates the focal mechanism solution, aftershock relocation, and GPS and leveling data to reveal the coseismic fault and seismotectonics of the 2013 Lushan earthquake. Three-dimensional imaging of the aftershocks is used to identify two planar faults that form a Y-shape (f1 and f2). The main active fault f1 dips to the northwest at approximately 45°–50° at depths of 7–19 km. Seismic interpretations suggest that it did not break through the overlying Mesozoic and Cenozoic rocks, and also that it is a blind fault. Geodetic measurements suggest that the coseismic deformation is consistent with the geometry and kinematics of shear fault-bend folding. The deep seismic reflection profile indicates that the syndepositional nature of the fault is a pre-existing normal fault older than the Triassic that underwent positive inversion tectonics during the Late Cenozoic. The 2013 Lushan earthquake, which was triggered by blind faults, is deemed to be a hidden earthquake. Blind and reactivated faults increase the potential risk and uncertainty related to earthquakes in the eastern margin of the Tibetan Plateau.

R.-Q. Lu (✉) · X.-B. Tan · Y.-Q. Li · Z.-N. Wang
State Key Laboratory of Earthquake Dynamics, Institute of Geology, China Earthquake Administration, Beijing, China
e-mail: Lurq127@sina.com

X.-W. Xu
Institute of Crustal Dynamics, China Earthquake Administration, Beijing, China

D.-F. He
College of Energy Resources, China University of Geosciences, Beijing, China

J. Suppe
Department of Earth and Atmospheric Sciences, University of Houston, Houston, TX, USA

5.1 Introduction

On April 20, 2013, an unexpected M_w 6.7 earthquake occurred in Lushan County at the southern side of Longmen Shan (LMS). The hypocenter of this earthquake was located approximately 80 km southwest of the 2008 Wenchuan earthquake (Fig. 5.1). Both earthquakes resulted in a large number of casualties and losses [36, 37]. Some studies have suggested that the seismogenic fault was a high-angle listric-reverse fault that is probably linked to the Shuangshi-Dachuan fault (F4) [4]; however, a field
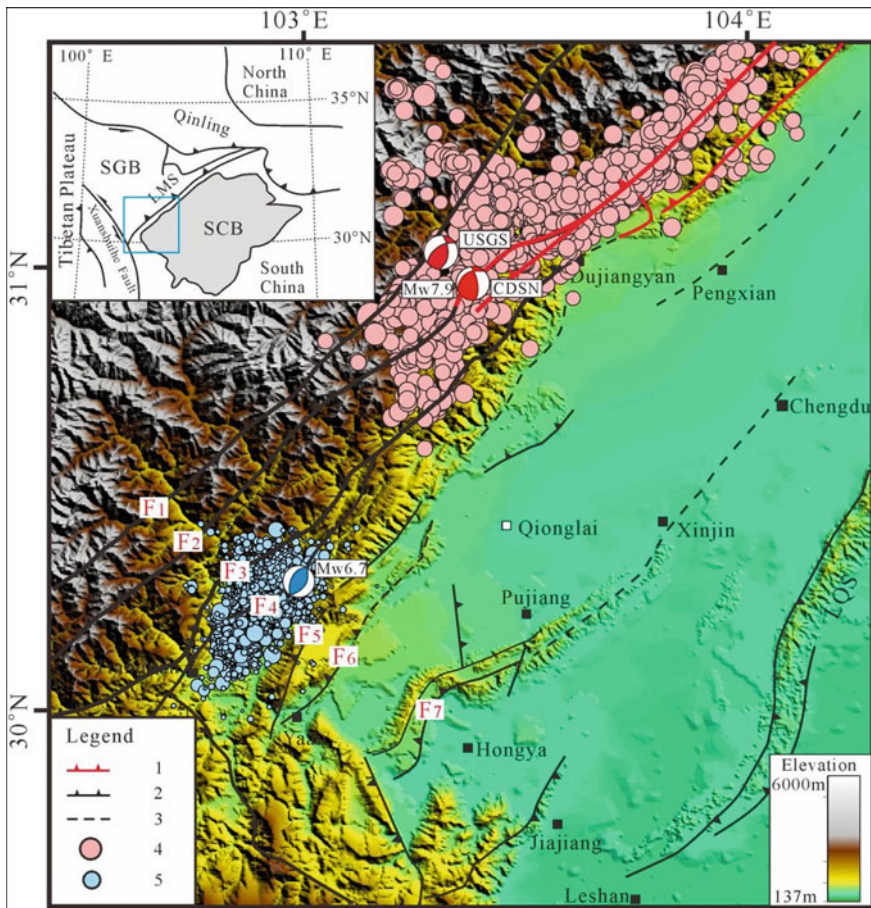

Fig. 5.1 The major fault system and earthquakes in the southern LMS thrust belt. The black solid lines represent the major faults and the dashed lines represent the blind or concealed faults

investigation did not find coseismic surface ruptures [16] and did not support the idea that F4 is the seismogenic fault. Seismic and geological interpretations suggest that the seismogenic fault is a gently dipping frontal blind thrust at an approximate angle of 30° [17, 33]; however, the relocated aftershocks and focal mechanism solution indicate that the seismogenic fault dips at ~7° to the northwest [9, 41]. In addition, other geological studies have suggested that the Lushan earthquake was caused by thrusting and detachment folding in the frontal propagation belt of the LMS [21] and that the seismogenic fault was the Dayi fault (F6) in the frontal mountain [18]. Moreover, geodetic measurements, including GPS and leveling data obtained during the earthquake, suggest a maximum coseismic displacement in the Lushan syncline area [10, 14]. Furthermore, the coseismic deformation of the Lushan earthquake is not consistent with the tectonics and geomorphology of the shallow sediments and as such there is an ongoing debate regarding the location, geometry, and kinematics of the Lushan seismogenic fault [22].

Presently, there are many uncertainties concerning the disastrous earthquakes in the LMS area [39]. For example, calculations of the Coulomb stress variations suggest that the previously accumulated stress was not completely released by the Wenchuan M$_w$ 7.9 and Lushan M$_w$ 6.7 earthquakes [6, 24]. Previous studies have warned that the LMS fault zone is active and presents a high risk [1] and thus, following a devastating seismic event, it is critical to determine where and when the next big earthquake will occur. Therefore, it is increasingly important to urgently survey active faults and assess potential seismic risks in the LMS area. Solving these problems is critical to understanding the seismogenic fault and seismotectonics of the Lushan earthquake and then to estimate the potential seismic hazard along the eastern margin of the Tibetan Plateau.

Legend: 1. Coseismic surface rupture of the Wenchuan earthquake; 2. Major faults; 3. Blind faults; 4. Aftershocks of the Wenchuan M$_w$ 7.9 earthquake; 5. Aftershocks of the Lushan M$_w$ 6.7 earthquake; F1. Longdong fault; F2. Wulong fault; F3. Xiaoguanzi fault; F4. Shuangshi-Dachuan fault; F5. Xinkaidian fault; F6. Dayi blind fault; F7. Sansuchang fault; SGB: Songpan–Ganze Block; LMS: Longmen Shan; SCB: Sichuan Basin; LQS: Longquan Shan.

5.2 Geological Setting

The approximately 500 km long and 30–50 km wide LMS thrust belt forms the eastern margin of the Tibetan Plateau (Fig. 5.1). The belt defines a sharp topographic transition between the Songpan–Ganze Block (SGB) and the Sichuan Basin (SCB) [2], which is a known seismically active area with complex intracontinental deformation [7, 15].

The LMS area has a long and complex tectonic history and its three main deformation stages since the Paleozoic have been identified [5, 19]. A number of extensional events occurred in the western SCB and LMS during the Paleozoic to Middle Triassic [23] that resulted in the formation of normal faults. Since the Mesozoic, the LMS

thrust belt has had two major periods of contractional deformation, specifically in the late Triassic and the Cenozoic [13]. During the late Triassic, the tectonic setting changed from a rifted passive margin to a foreland in response to the final closure of the Paleo-Tethys and the continent–continent collisions of the North China, South China, and Qiangtang blocks [2]. During the Cenozoic, tectonism in the LMS was reactivated as a result of the India–Asia continental collision [30] and manifested in thrusting, dextral shear, uplifting, and exhumation [8].

The LMS area currently comprises a series of northeast-trending thrust faults [2, 19, 22]. The Wenchuan earthquake occurred in the central LMS and produced two large surface ruptures along the major faults (Fig. 5.1). The southern LMS thrust belt is distinguishable by the Longdong fault (F1), the Wulong fault (F2), the Xiaoguanzi fault (F3), and the Shuangshi-Dachuan fault (F4). The deformation in the western SCB is characterized by imbricated thrusts and fault-related folds (Fig. 5.2). The Lushan earthquake occurred in the southern LMS, but field investigations have not revealed any evidence of surface rupture due to this earthquake [16, 37].

The outcrops of the southern LMS are mainly Mesozoic strata (Fig. 5.2). This area is characterized by Baoxing complex rocks. Surface geological and drilling data indicate that the shallow sedimentary cover of the southern LMS contains mainly Sinian–Middle Triassic shallow marine clastic and carbonate rocks and late Triassic
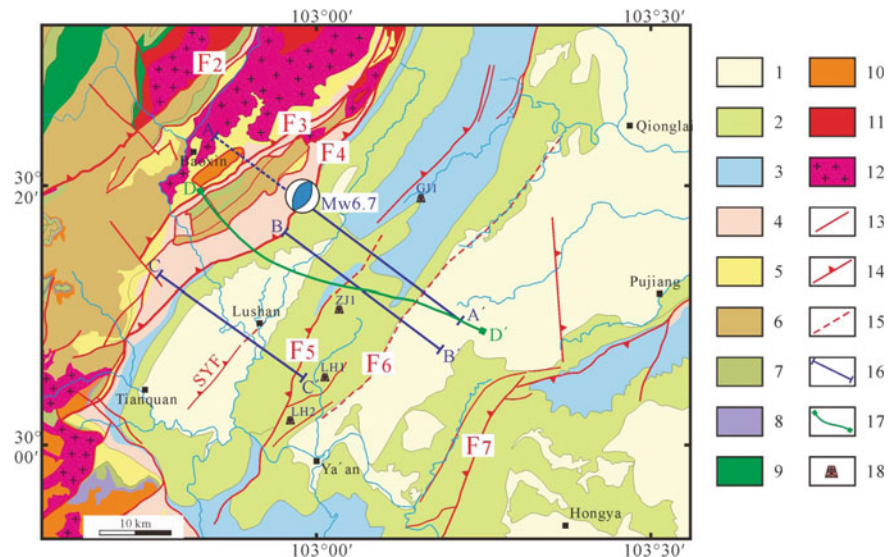

Fig. 5.2 Geology and location of artificial seismic reflection profiles in the research area. Legend: 1. Cenozoic; 2. Cretaceous; 3. Jurassic; 4. Triassic; 5. Permian; 6. Devonian; 7. Silurian; 8. Ordovician; 9. Cambrian; 10. Sinian; 11. Proterozoic; 12. Complex rocks; 13. Major faults; 14. Thrusts; 15. Blind faults; 16. Artificial seismic reflection profile; 17. Deep seismic reflection profile; 18. Drilling wells. SYF: Shiyang fault

non-marine clastics (Fig. 5.3). An early Proterozoic crystalline basement lies under this sedimentary cover.

There is an important shallow-level detachment (D1) that developed within the lower-Middle Triassic gypsum layers [13, 22]. This shallow detachment fault slips toward the foreland basin and forms the LQS anticline [20]. In addition, a potential deep-level detachment (D2) exists in the pre-Sinian crystalline basement beneath
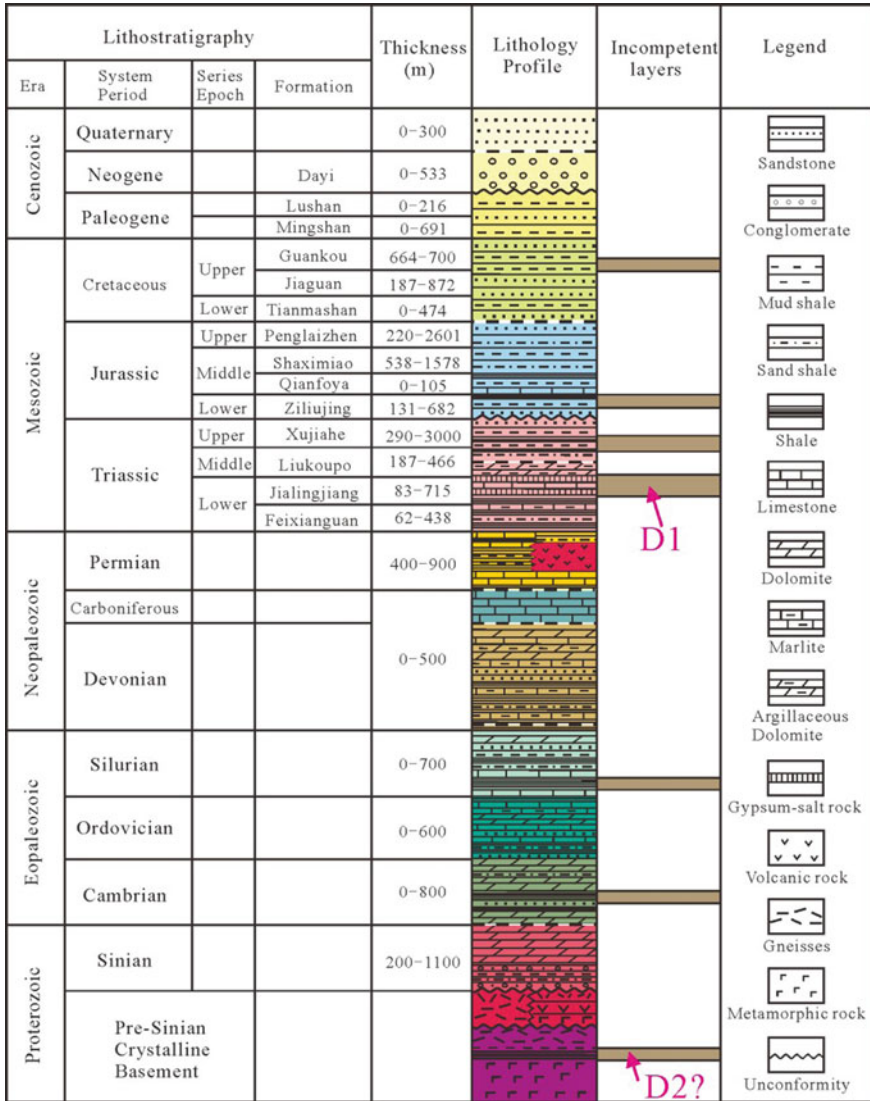

Lithostratigraphy				Thickness (m)	Lithology Profile	Incompetent layers	Legend
Era	System Period	Series Epoch	Formation				
Cenozoic	Quaternary			0–300			Sandstone
	Neogene		Dayi	0–533			
	Paleogene		Lushan	0–216			Conglomerate
			Mingshan	0–691			
Mesozoic	Cretaceous	Upper	Guankou	664–700			Mud shale
			Jiaguan	187–872			
		Lower	Tianmashan	0–474			
	Jurassic	Upper	Penglaizhen	220–2601			Sand shale
		Middle	Shaximiao	538–1578			
			Qianfoya	0–105			
		Lower	Ziliujing	131–682			Shale
	Triassic	Upper	Xujiahe	290–3000			
		Middle	Liukoupo	187–466			
		Lower	Jialingjiang	83–715		D1	Limestone
			Feixianguan	62–438			
Neopaleozoic	Permian			400–900			Dolomite
	Carboniferous			0–500			Marlite
	Devonian						Argillaceous Dolomite
Eopaleozoic	Silurian			0–700			Gypsum-salt rock
	Ordovician			0–600			Volcanic rock
	Cambrian			0–800			Gneisses
Proterozoic	Sinian			200–1100			Metamorphic rock
	Pre-Sinian Crystalline Basement					D2?	Unconformity

Fig. 5.3 Histogram of the regional stratigraphy of the LMS and the western SCB

the southeastern region of the Tibetan Plateau [31, 38]. Multiple detachments and superimposed deformation events are characteristic features of the southern LMS.

5.3 Shallow Structural Deformation

There are three typical seismic reflection profiles in the Lushan earthquake area (Figs. 5.2 and 5.4). We can determine the shallow geological and structural characteristics of the study area from the seismic interpretation of these profiles. The Dayi blind fault (F6) developed on the shallow D1, which is located in the Mid–Lower Triassic strata (Fig. 5.4a), but the Xinkaidian fault (F5) and the Shiyang fault (SYF) developed on a shallower detachment in the Jurassic strata (Fig. 5.4b, c).

In profiles A and B (Fig. 5.4a, b), there is a large anticline beneath the Lushan area. This anticline deformed the D1 and the Mesozoic strata. A previous study interpreted this as a fault-bend fold, and our seismic interpretations were consistent with this previous model [13]. The anticline was formed by a fault-bend folding (FBF) and developed a black thrust. The lower detachment D2 was only inferred from the axial surfaces and structural deformations.

Although the shallow sedimentary and structural deformation of the southern LMS does not reveal the information directly [22], it provides important constraints on the seismotectonics of the 2013 Lushan earthquake.

5.4 3D Coseismic Fault Model

Previous studies have used aftershocks from large earthquakes to model faults by fitting the three-dimensional (3D) surfaces to earthquake clusters using the Gocad software [3]. The approximately 2,000 events (Fig. 5.5a) of the Lushan earthquakes were relocated using the double-difference method [9]. Parallel to the strike of the LMS thrust belt (Fig. 5.5b), most of the hypocenters were confined to a depth range between 7 and 19 km. In addition, the northwest-dipping earthquake cluster intersected the southeast-dipping earthquake cluster and both formed a Y-shape. The relocated aftershocks suggest the presence of at least two coseismically active faults. According to the distribution of the aftershocks, the 3D geometry of the coseismic faults was mapped successfully [21].

The aftershock hypocenters of the Lushan earthquake and the 3D images of the seismogenic fault surfaces were produced using the SKUA-Gocad software (Fig. 5.5c). We used the aftershock hypocenter locations of the Lushan earthquake to image the active faults in detail. Figure 5.5c, d shows the same view direction with a 15° plunge angle and a 35° strike.

The 3D depth-contoured surfaces illustrate the detailed geometry of faults f1 and f2 (Fig. 5.5d). The surfaces of these faults are inhomogeneous and contain multiple
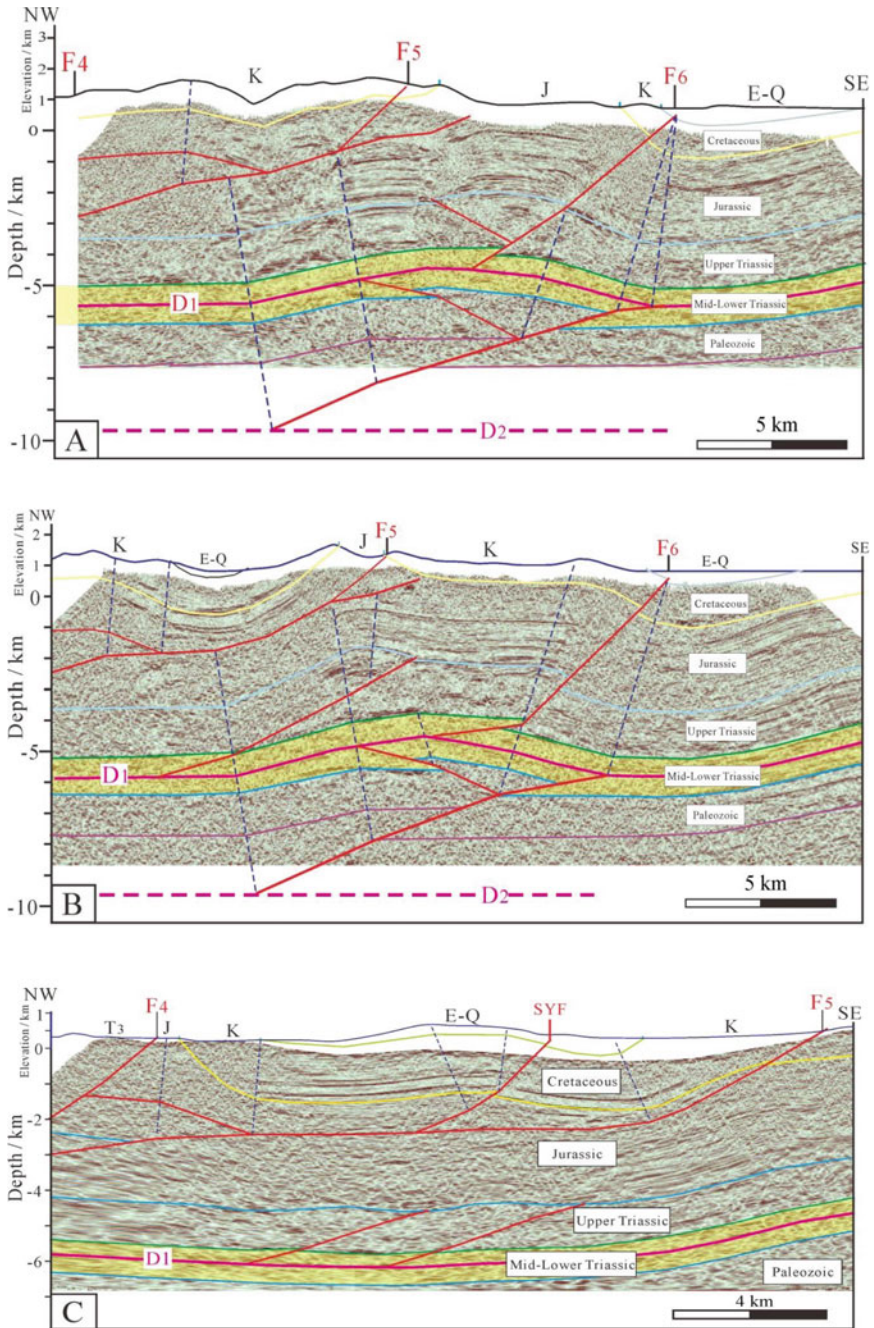
Fig. 5.4 Geological and structural interpretation of the seismic reflection profiles A, B, and C. The yellow area represents the Mid–Lower Triassic and detachment layer (D1). The red solid lines represent the faults and the black dashed lines represent the axial surfaces
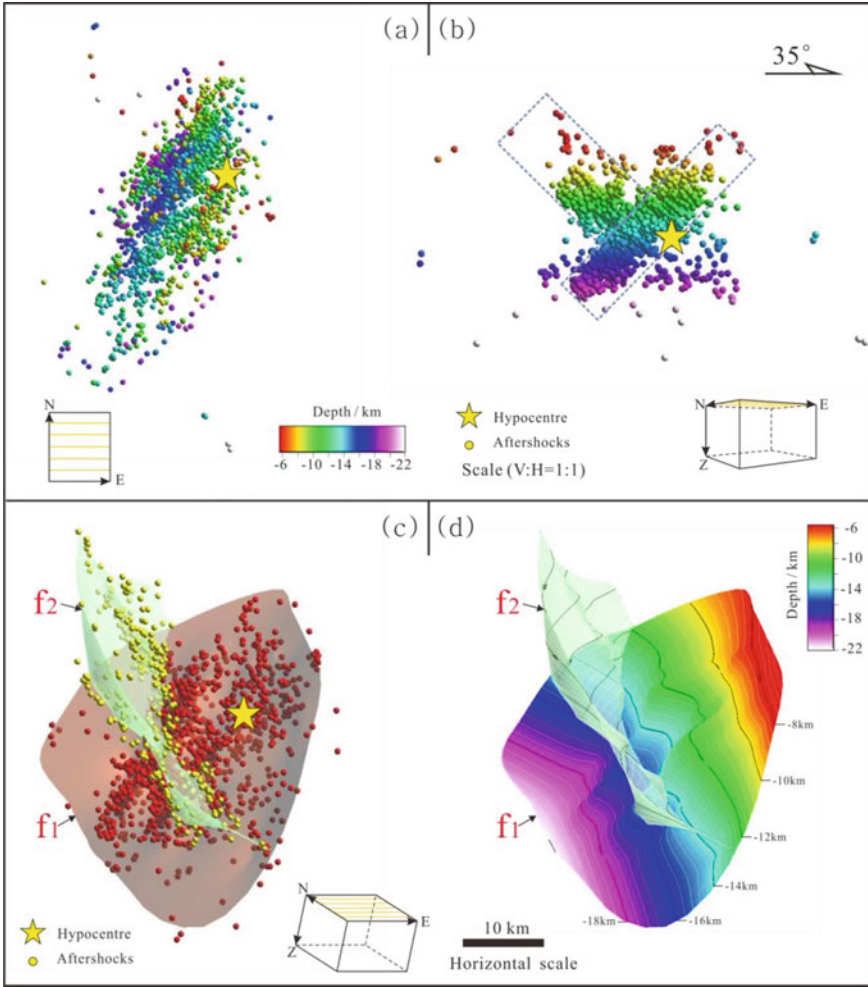
Fig. 5.5 Imaging the 3D geometry of the coseismic faults using the SKUA-Gocad software. **a** Map view of the aftershock hypocenters. **b** View parallel to the strike; the strike direction of the aftershocks is ~55°. **c** 3D images of the ruptured fault surfaces modeled based on the aftershock hypocenters after smoothing with the Gocad DSI algorithm. **d** Depth-contoured surfaces of the ruptured faults. The coordinate system is WGS 84 UTM 48 in the northern hemisphere. Approximately 2,000 relocated aftershocks were used ($M \geq 1.0$)

wave bends. Fault f1 is the major seismogenic fault of the Lushan earthquake and has a 45°–50° dip, whereas fault f2 is a branching backthrust of f1.

5.5 Seismic Interpretation and Quantitative Analysis

Profile E–E′ is a high-resolution petroleum industry seismic reflection profile between the southern LMS and western SCB (Fig. 5.6). This profile crosses the major fault-folding belt, and provides information on the shallow sediments and structures from the subsurface down to a depth of ~10 km. The Lushan syncline lies between the F4 and Xinkaidian fault (F5) (Figs. 5.1 and 5.2) and the hypocenter of the Lushan earthquake is beneath the F4 at a depth of 12–13 km [9, 41].
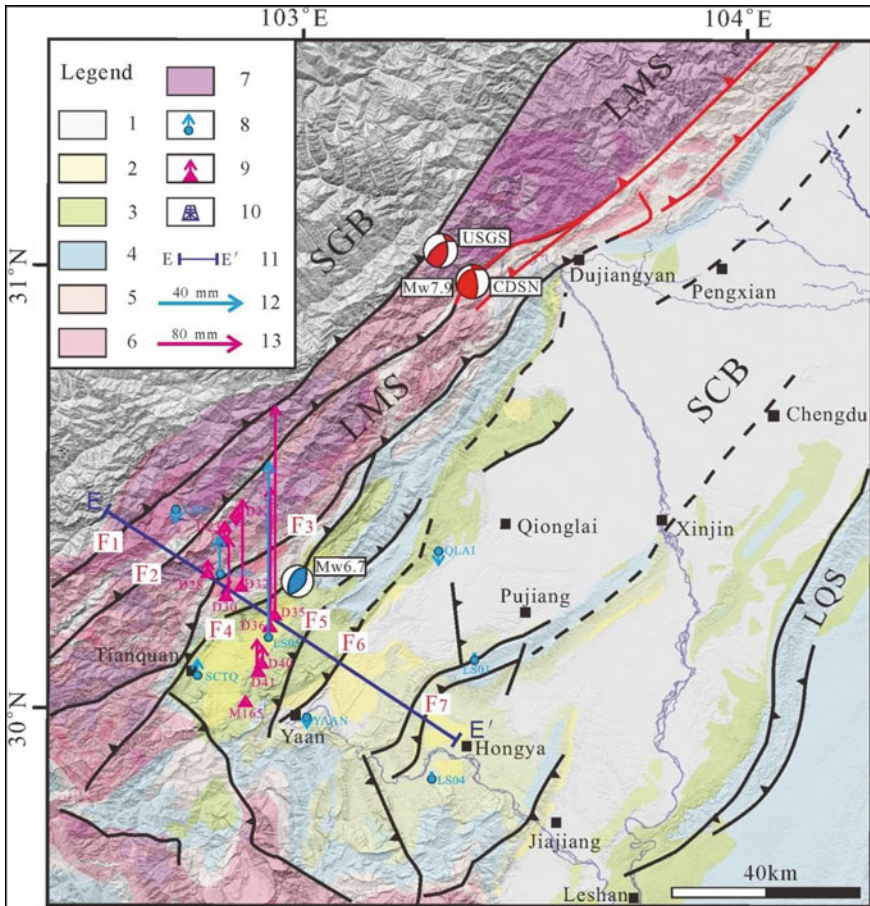
Fig. 5.6 Geological map of the southern LMS with the locations of the artificial seismic reflection profile, drilling wells, and GPS and leveling stations described in this study. Legend: 1. Quaternary; 2. Paleogene; 3. Cretaceous; 4. Jurassic; 5. Triassic; 6. Paleozoic; 7. Proterozoic and complex rocks; 8. GPS stations and measurements; 9. Leveling stations and measurements; 10. Drilling wells; 11. Petroleum industry seismic reflection profile; 12. Scale for GPS data [14]; and 13. Scale for leveling data [10]

In this seismic profile (Fig. 5.7), the labels on each layer denote certain seismic reflectors in the sediment rather than stratigraphic boundaries. The seismic reflectors in the Lushan syncline area are clear and continuous, suggesting that no thrust faults extend into the syncline; however, the partially enlarged portion of the seismic profile clearly shows the deformation features on top of the aftershock cluster (Fig. 5.7E1). The seismic reflectors of the Lower Paleozoic units are discontinuous and may suggest the presence of a fault that cuts across the Lower Paleozoic and some Upper Paleozoic layers [21]. The location of this fault is consistent with the location of the 3D-mapped seismogenic fault f1 (Fig. 5.5). Obviously, it has not broken through the Upper Triassic strata and is possibly a blind fault.

The seismic reflection profile E–E' is ~11 km away from the Lushan M_w 6.7 mainshock. Section E1 displays a detailed seismic reflection image of the deformation features and strong seismic reflectors. It shows aftershocks for a range of ~4 km. The green arrows indicate the characteristics of the same layers. Section E2 shows the quantitative angle measurement of the fault f3. The geometry of faults f1 and f2 was simplified from the 3D images.

FBF: Fault-bend folding (the simple shear FBF model II was modified from [40]). D1: shallow-level detachment; D2: possible deep-level detachment. The black dashed lines represent the axial surfaces and some speculated faults are shown as red dashed lines.
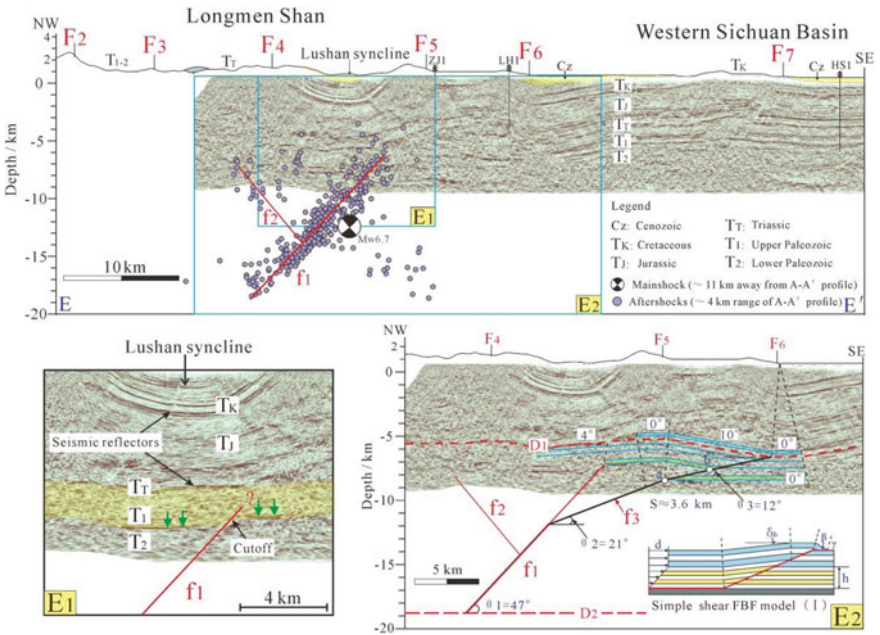

Fig. 5.7 Comprehensive analysis of the high-resolution seismic reflection profile E–E'

The detachments at the various levels may play a prominent role in the LMS and western SCB (Fig. 5.3). Some shallow detachments are parallel to the sedimentary layers and lead to shallow structural deformation [20]. Some detachments have propagated into the western SCB and produced fault-related folds during the Cenozoic, such as the Longquan Shan (LQS) anticline and Xiongpo anticline [12, 17, 33]. The seismic interpretation of profile E–E′ suggests that a shallow D1 occurs in the Mid–Lower Triassic gypsum beds. Some Mesozoic- and Cenozoic-age thrusts have developed on this detachment in the western SCB (Figs. 5.3 and 5.7E2). According to the S-wave velocity structure and structural analysis, a deep D2 is inferred to exist in the basement rocks at a depth of ~20 km [32]; however, the D2 may not be a regular horizontal surface at an accurate depth. Based on the distribution of the Lushan aftershocks and the seismic interpretation (Figs. 5.5 and 5.7), the D2 was determined to be located at a depth of approximately 19 km in this profile.

Between detachments D1 and D2, there is a large anticline beneath the F5 (Fig. 5.7), which is similar to the three shallow seismic profiles (Fig. 5.4). The f1 and f2 faults were simplified as two straight lines from the 3D images (Fig. 5.5). A main thrust fault f3 cuts the basement and merges with D1. We measured the dips of the layers and calculated the dip of fault f3 using the classical FBF theory [28]. The accumulated slip of fault f3 is ~3.6 km (Fig. 5.7E2). The seismic profile indicates that the f3 fault cuts the layers beneath D1 with a cutoff angle (θ3) of 12°. The cutoff angle θ2 is ~21° and fault f3 likely converges with fault f1 at a depth of ~12 km [21]. There is no evidence to show that the basal layer slides shorten and thicken above the ramp. The D2 detachment layer undergoes contraction and has a simple bedding-parallel surface with no basal fault slip but the layers above the ramp have no bedding-parallel surface. The geometry of fault f3 and the analysis of the axial surfaces suggest that the structure of f3 is consistent with the shear FBF model, which is characterized by long, gentle back limbs that dip less than the fault ramp [29].

Geodetic crustal displacement data is important for the study of active tectonics [27, 34], and can provide independent constraints for fault kinematics, particularly when no surface rupture features are available [14]. The GPS and leveling data collected during the 2013 Lushan earthquake indicate that the maximum coseismic deformations occurred in the Lushan syncline area (Fig. 5.8). In particular, at GPS station LS05 located ~15 km south of the epicenter an ~68 mm horizontal displacement and ~84 mm uplift were observed (Fig. 5.8E3). The angle of the coseismic deformation was approximately 50°, which is similar to the dip of fault f1. The leveling data suggest that the maximum coseismic displacements appeared at station D35 (Fig. 5.8E4) with an uplift of ~198.4 mm [10].

Section E3 shows the geological and structural interpretation of the seismic section in Fig. 5.7E2. The coseismic deformation obtained from the GPS data is shown at the top. The simple shear FBF model II was modified from [29]. Section E4 shows the geometry and kinematics model of seismogenic fault f1. The coseismic deformation of the leveling data is displayed above fault f1. Layer 1 indicates the deformation and the total uplift area, which are similar to the coseismic deformation of the leveling data.
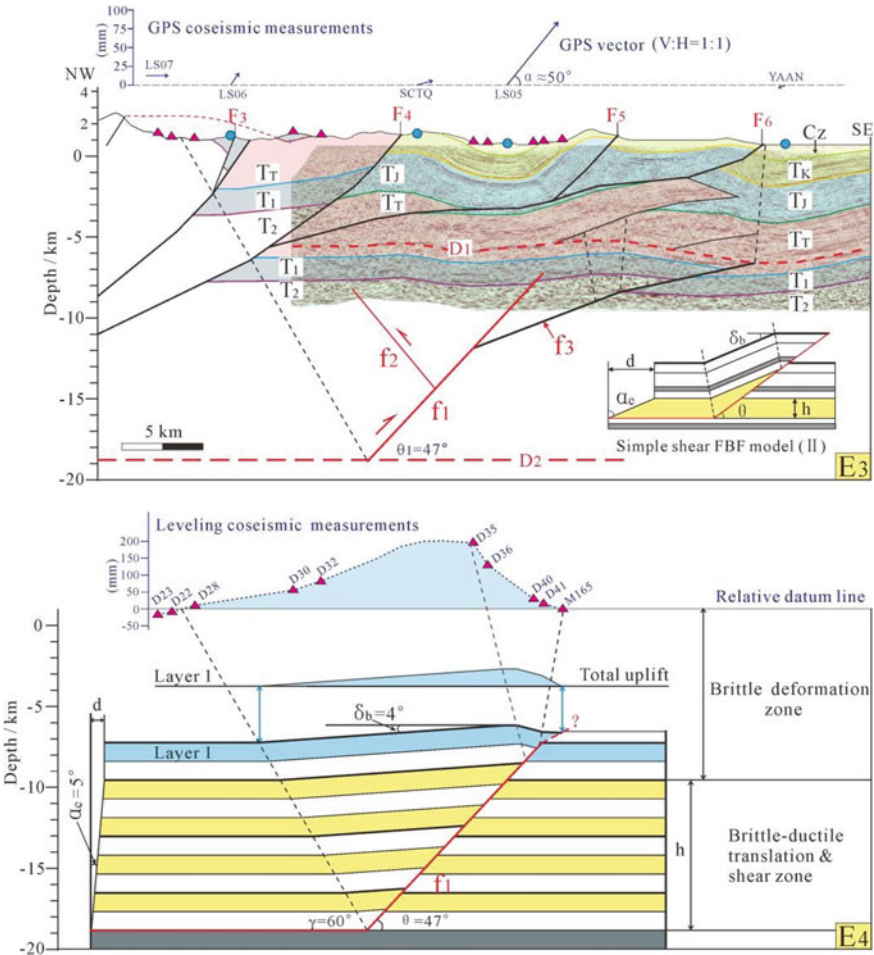
Fig. 5.8 Quantitative analysis of the geometry and kinematics of the seismotectonics of the 2013 Lushan earthquake

In this study, we mapped the area of the uplift resulting from the coseismic deformation and found that it has broad limb rotation in the back limb (Fig. 5.8E4). The back-dip (δb) measured from the seismic reflection profile is 4° and the ramp dip ($\theta 1$) is 47°. According to the simple shear FBF model and relevant formulae [26, 29], the shear angle (αe) is ~5°. The instantaneous kinematics and total uplift of the coseismic deformations indicate that the seismotectonics of the Lushan earthquake correlate with the simple shear FBF model [40], which successfully explains the back limb uplift [21]. This result suggests that the upper crust in the study area has a brittle deformation zone above ~10 km and a brittle–ductile translation or shear zone between 10 and 20 km. This brittle–ductile translation zone is consistent with the results of previous studies [32, 38].

5.6   Seismotectonics of the Lushan Earthquake

A deep seismic reflection profile D–D′ was collected following the 2013 Lushan earthquake (Fig. 5.2). This seismic profile shows the image of a deep structure beneath the Lushan syncline (Fig. 5.9). The seismic reflectors suggest that the Triassic and some Upper Paleozoic layers are roughly continuous [21], which is consistent with the other profiles (Figs. 5.4 and 5.7). However, the Lower Paleozoic layers exhibit a prominent offset above the mainshock of the Lushan earthquake, which suggests the presence of a fault cutting the Lower Paleozoic and basement rocks.

The focal mechanism of the 2013 Lushan earthquake suggests that the seismogenic fault f1 is a thrust fault (Fig. 5.1). However, the deep seismic profile D–D′ shows that it is a typical normal fault, as there are thin layers in the footwall of f1 but thick sediments in the hanging wall between the Upper Paleozoic and Lower Paleozoic units (Fig. 5.9). These syndepositional features formed in response to the growth of fault f1. Based on the tectonic evolution of the LMS [19, 23], we suggest that fault f1 was a normal fault during the Paleozoic (Fig. 5.9D1).

The seismogenic fault f1 involves positive inversion tectonics. It is just starting to form (Fig. 5.9D2); however, as it has not broken through the postrift strata, as
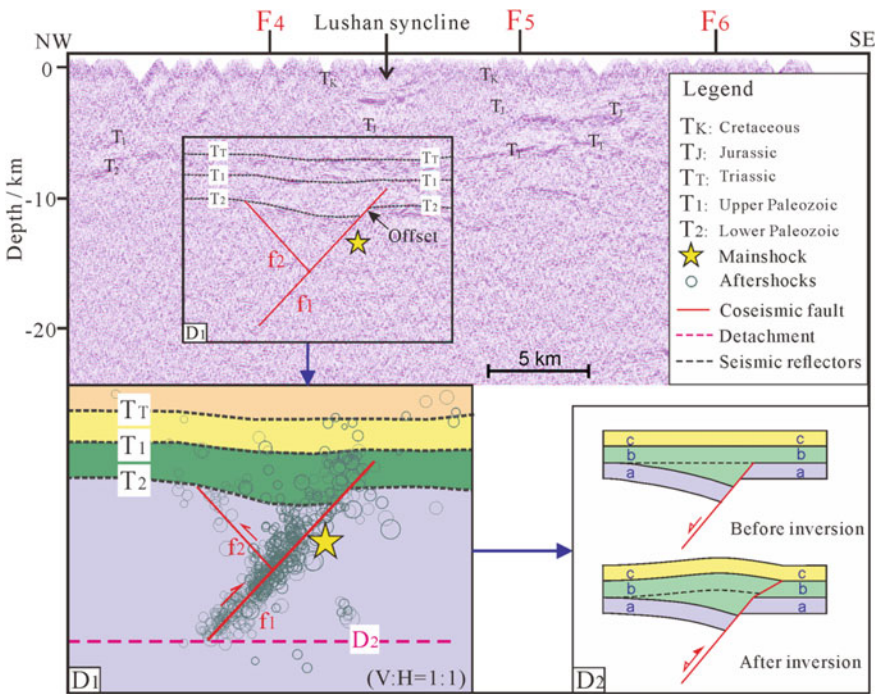

Fig. 5.9 Deep artificial seismic reflection profile D–D′ and the coseismic faults of the Lushan earthquake

positive inversion structural evolution models suggest [35], and has barely caused any structural deformations. Fault f3 is the main fault with a slip at ~3.6 km (Fig. 5.7E2), which suggests that it formed and tectonically inverted during the Late Cenozoic.

In this figure, the seismically active f1 and f2 faults are simplified as two straight lines. Section D1 shows the coseismic faults and the geological model of the 2013 Lushan earthquake, suggesting that fault f1 was a normal fault prior to the Mesozoic period. Section D2 shows the schematic of a classical positive inversion structure. The stratigraphic sequences "a", "b", and "c" are prerift, synrift, and postrift, respectively (modified from [35]).

Previous studies demonstrated the formation of several normal faults prior to the Late Triassic period in the LMS area [2, 13]. Since the Cenozoic, some pre-existing syndepositional normal faults facilitated the structural inversion that transformed them into thrust faults in a compressional regime [5]. In the LMS area and the western SCB, several of these pre-existing normal faults were structurally inverted and transformed into active thrust faults in a contractional setting [7, 30].

Clearly, the seismotectonics of the 2013 Lushan M_w 6.7 earthquake are different from the seismotectonics of the 2008 Wenchuan M_w 7.9 earthquake (Fig. 5.10). The Wenchuan earthquake ruptured the upper crust with two main faults in the LMS [36], but the seismogenic fault f1 responsible for the 2013 Lushan earthquake is a blind fault that was reactivated during the Late Cenozoic [22]. It also differs from the 2016 M_w 6.4 Meinong earthquake in Taiwan, which was triggered by a blind thrust fault with fault propagation folds [11]. Both faults f1 and f3 were developing but did not break through the shallow detachment D1. Therefore, we suggest that the Lushan earthquake activity on the seismogenic fault f1 is a hidden earthquake [25].
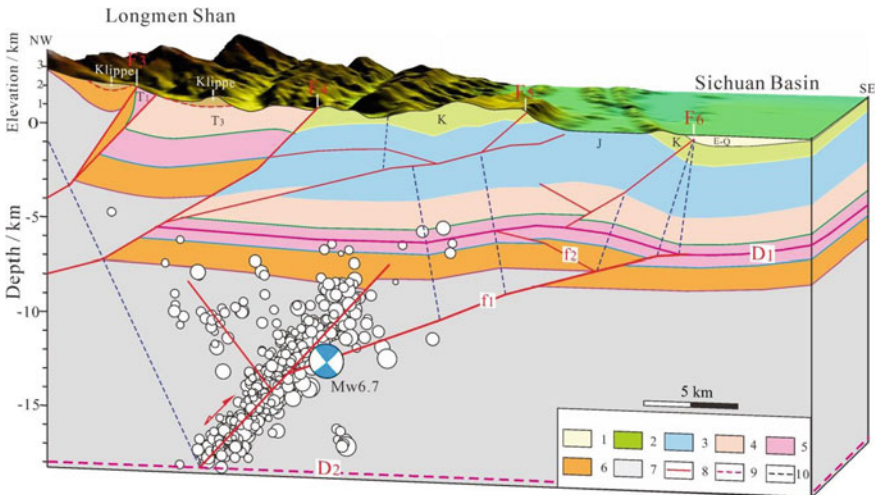

Fig. 5.10 A 3D geological and structural model showing seismotectonics of the Lushan earthquake. Legend: 1. Cenozoic; 2. Cretaceous; 3. Jurassic; 4. Upper Triassic; 5. Mid–Lower Triassic; 6. Upper Paleozoic; 7. Pre-Cambrian and basement; 8. Major faults; 9. Main detachments; 10. Axial surfaces

It is known that many active and blind faults exist in the frontal LMS and western SCB [33]; furthermore, several scientists believe that the accumulation of strain energy in the southern LMS area was not completely released by the 2013 Lushan event [6]. The seismotectonics of the 2013 Lushan earthquake show that inversion tectonics could trigger a strong earthquake, and these were an important factor in the development of the southern LMS during the Late Cenozoic. Furthermore, the blind fault led to a hidden earthquake, which suggests that the frontal ramp of these reactivated faults poses a potential seismic risk. With the ongoing compression of the Tibetan Plateau toward the western SCB during the Late Cenozoic [42], the level of seismic risk in the LMS and western SCB area is increasingly uncertain.

5.7 Conclusions

The 2013 M$_w$ 6.7 event was a hidden earthquake that was ruptured by an unknown blind thrust fault in the frontal Longmen Shan (LMS). Three-dimensional imaging of the aftershocks was used to identify two planar faults that form a Y-shape with the major seismogenic fault f1 dipping to the northwest at 45°–50° at a depth of 7–19 km. Seismic interpretations suggest that the seismogenic fault is a typical blind fault that did not penetrate into the overlying Mesozoic and Cenozoic units and it is not a Shuangshi-Dachuan fault (F4) or a frontal Dayi buried fault (F6). Deep seismic data illustrate the syndepositional characteristics of the seismogenic fault. Our study further demonstrated that the seismogenic slip occurred on a reactivated pre-existing normal fault older than the Triassic age that triggered earthquakes during the Late Cenozoic.

There are two major detachments that control the structural deformation of the upper crust in the LMS and western Sichuan Basin (SCB), resulting in multiple superimposed deformation events. Based on the structural and coseismic deformation, we argue that the main seismotectonics of the Lushan earthquake are consistent with the simple shear fault-bend folding model. Clearly, the 2013 Lushan earthquake was not a characteristic earthquake. Due to the strong compression of the Tibetan Plateau toward the SCB, the early-period normal faults were activated after inversion and triggered the Lushan earthquake. The concealed and reactivated faults increase the potential risks related to earthquakes in the LMS and the western SCB.

References

1. Broadbent N (2014) Longman shan fault zone still hazardous, suggest new reports. Seismol Res Lett http://www.eurekalert.org/pub_releases/2014-01/ssoa-lfz122513.php
2. Burchfiel BC, Chen Z, Liu Y, Royden LH (1995) Tectonics of the Longmen Shan and adjacent regions, central China. Int Geol Rev 37:661–735. https://doi.org/10.1080/00206819509465424
3. Carena S, Suppe J (2002) Three-dimensional imaging of active structures using earthquake aftershocks: the Northridge thrust, California. J Struct Geol 24:887–904
4. Chen LC, Wang H, Ran YK, Lei SK, Li X, Wu FY, Ma XQ, Liu CL, Han F (2014) The 2013 Lushan Ms 7.0 earthquake: varied seismogenic structure from the 2008 Wenchuan earthquake. Seismol Res Lett 85:34–39. https://doi.org/10.1785/0220130109
5. Chen SF, Wilson CJL (1996) Emplacement of the Longmen Shan thrust-nappe belt along the eastern margin of the Tibetan Plateau. J Struct Geol 18:413–430
6. Chen YT, Yang ZX, Zhang Y, Liu C (2013) From 2008 Wenchuan earthquake to 2013 Lushan earthquake. Scientia Sinica Terrae 43:1064–1072
7. Deng QD, Chen SF, Zhao XL et al (1994) Tectonics, seismicity and dynamics of Longmen Shan mountains and its adjacent regions (in Chinese). Seismol Geol 16(4):389–403
8. Densmore AL, Ellis MA, Li Y, Zhou RJ, Hancock GS, Richardson N (2007) Active tectonics of the Beichuan and Pengguan faults at the eastern margin of the Tibetan Plateau. Tectonics 26, TC4005
9. Fang LH, Wu JP, Wang WL, Du WK, Su JR, Wang CZ, Yang T, Cai Y (2015) Aftershock observation and analysis of the 2013 Ms 7.0 Lushan earthquake. Seismol Res Lett 86:1–8. https://doi.org/10.1785/0220140186
10. Hao M, Wang QL, Liu LW, Shi Q (2014) Interseismic and coseismic displacements of the Lushan Ms7.0 earthquake inferred from leveling measurements. Chin Sci Bull 59:5129–5135. https://doi.org/10.1007/s11434-014-0652-4
11. Huang MH, Tung H, Fielding E, Huang HH, Cunren L, Chuang H, Hu JC (2016) Multiple fault slip triggered above the 2016 Mw 6.4 MeiNong earthquake in Taiwan. Geophys Res Lett. https://doi.org/10.1002/2016gl069351
12. Hubbard J, Shaw JH (2009) Uplift of the LMS and Tibetan Plateau, and the 2008 Wenchuan (M = 7.9) earthquake. Nature 458:194–197. https://doi.org/10.1038/nature07837
13. Jia D, Wei GQ, Chen ZX, Li BL, Zeng Q, Yang G (2006) Longmen Shan fold-thrust belt and its relation to western Sichuan Basin in central China: new insights from hydrocarbon exploration. Am Assoc Petrol Geol 90:1425–1447. https://doi.org/10.1306/03230605076
14. Jiang ZS, Wang M, Wang YZ, Wu YQ, Che S, Shen ZK, Bürgmann R, Sun JB, Yang YL, Liao H, Li Q (2014) GPS constrained coseismic source and slip distribution of the 2013 Mw6.6 Lushan, China, earthquake and its tectonic implications. Geophys Res Lett 41:407–413
15. Kirby E, Whipple K, Harkins N (2008) Topography reveals seismic hazard. Nat Geosci 1:485–487. https://doi.org/10.1038/ngeo265
16. Lei SX, Ran YK, Wang H et al (2014) Discussion on whether there are coseismic surface ruptures of the Lushan Ms7.0 earthquake at Longmen area and its implications (in Chinese). Seismol Geol 36(1):266–274
17. Li Y, Jia D, Wang M, Shaw JH, He J, Lin A, Xiong L, Rao G (2014) Structural geometry of the source region for the 2013 Mw 6.6 Lushan earthquake: implication for earthquake hazard assessment along the Longmen Shan. Earth Planet Sci Lett 390:275–286. https://doi.org/10.1016/j.epsl.2014.01.018
18. Li Y, Zhou RJ, Zhao GH et al (2013) Thrusting and detachment folding of Lushan earthquake in front of Longmenshan Mountains (in Chinese). J Chendu Univ Technol 40(4):353–363
19. Liu SG (1993) The formation and evolution of Longmengshan thrust zone and Western Sichuan, China (in Chinese). Press of Chengdu University of Science and Technology, Chengdu, pp 17–117
20. Lu RQ, He DF, Xu XW et al (2016) The basement structures beneath the Central segment of Longmen ShanShan: constraints on the uplifting in the southeast margin of Qinghai-Tibet Plateau since the Cenozoic. J Asian Earth Sci 117:73–81

21. Lu RQ, Xu XW, He DF et al (2017) Seismotectonics of the 2013 Lushan Mw 6.7 earthquake: inversion tectonics in the eastern margin of the Tibetan Plateau. Geophys Res Lett 44:8236–8243
22. Lu RQ, Xu XW, He DF et al (2017) The shallow sedimentary and structural deformation in the southern Longmen Shan: constraints on the seismotectonics of the 2013 Lushan Mw6.7 earthquake. Chin J Geophys 60(8):2924–2934
23. Luo ZL, Jin YZ, Zhu KY, Zhao XK (1988) On Emei Taphrogenesis of the upper Yangze platform. Geol Rev 34:11–23
24. Parsons T, Ji C, Kirby E (2008) Stress changes from the 2008 Wenchuan earthquake and increased hazard in the Sichuan basin. Nature 454:509–510. https://doi.org/10.1038/nature07177
25. Stein RS, Yeats RS (1989) Hidden—earthquakes. Sci Am 260:48–57
26. Shaw JH, Connors C, Suppe J (2004) Seismic interpretation of contractional fault-related folds: an american association of petroleum geologists seismic atlas. Am Assoc Petrol Geol Spec Publ
27. Shen Zheng-Kang, Jianbao Sun, Zhang Peizheng (2009) Slip maxima at fault junctions and rupturing of barriers during the 12 May 2008 Wenchuan earthquake. Nat Geosci 2:718–724
28. Suppe J (1983) Geometry and kinematics of fault-bend folding. Am J Sci 283:684–721
29. Suppe J, Connors CD, Zhang YK (2004) Shear fault bend folding. In McClay KR (ed) Thrust tectonics and hydrocarbon systems, AAPG Memoir, vol 82, pp 303–323
30. Tapponnier P, Xu Z, Roger F, Meyer B, Arnaud N, Wittlinger G, Yang J (2001) Oblique stepwise rise and growth of the Tibet Plateau. Science 294:1671–1677. https://doi.org/10.1126/science.105978
31. Tang LJ, Yang KM, Jin WZ et al (2008) Multi-detachment and the structural deformation of Longmen mountain thrust belt. Sci China (in Chinese) 38:30–40
32. Wang CY, Lou H, Silver PG et al (2010) Crustal structure variation along 30° N in the eastern Tibetan Plateau and its tectonic implications. Earth Planet Sci Lett 289:367–376
33. Wang M, Jia D, Shaw JH, Hubbard J, Plesch A, Li Y, Liu BJ (2014). The 2013 Lushan earthquake: implications for seismic hazards posed by the range front blind thrust in the Sichuan Basin, China. Geology 42:915–918. https://doi.org/10.1130/G35809.1
34. Wang Qi, Qiao Xuejun, Lan Qigui (2011) Rupture of deep faults in the 2008 Wenchuan earthquake and uplift of the Longmen Shan. Nat Geosci 4:633–640
35. Williams GD, Powell CM, Cooper MA (1989) Geometry and kinematics of inversion tectonics. Geol Soc 44:3–15. https://doi.org/10.1144/GSL.SP.1989.044.01.02
36. Xu XW, Wen XZ, Yu GH, Chen GH, Klinger Y, Hubbard J, Shaw J (2009) Co-seismic reverse- and oblique-slip surface faulting generated by the 2008 Mw 7.9 Wenchuan earthquake, China. Geology 37(6):515–518. https://doi.org/10.1130/g25462a.1
37. Xu XW, Wen XZ, Han Z et al (2013) Lushan Ms7.0 earthquake: a blind reserve-fault earthquake (in Chinese). Chin Sci Bull 58. https://doi.org/10.1007/s11434-013-5999-4
38. Yan DP, Zhou MF, Li SB, Wei GQ (2011) Structural and geochronological constraints on the Mesozoic-Cenozoic tectonic evolution of the Longmen Shan thrust belt, eastern Tibetan Plateau. Tectonics 30:TC6005. https://doi.org/10.1029/2011tc002867
39. Yin A (2010) Preface: a special issue on the great 12 May 2008 Wenchuan earthquake (Mw7.9): observations and unanswered questions. Tectonophysics 491:1–9
40. Yue LF, Suppe J, Hung JH (2011) Two contrasting kinematic styles of active folding above thrust ramps, western Taiwan. In: McClay K, Shaw J, Suppe J (eds) Thrust fault-related folding. AAPG Memoir 94:153–186
41. Zeng XF, Luo Y, Han LB, Shi YL (2013) Lushan Ms7.0 earthquake on 20 April 2013: a high-angle thrust event. Chin J Geophys 56:1418–1421. https://doi.org/10.6038/cjg20130437
42. Zhang P, Shen Z, Wang M, Gan W, Burgmann R, Molnar P (2004) Continuous deformation of the Tibetan Plateau from global positioning system data. Geology 32:809–812